

Multi-Ring Deposition Pattern of Drying Droplets

Mengmeng Wu,^{1,2} Xingkun Man,^{1,2,*} and Masao Doi^{1,2}

¹*Center of Soft Matter Physics and its Applications,
Beihang University, Beijing 100191, China*

²*School of Physics and Nuclear Energy Engineering,
Beihang University, Beijing 100191, China*

Abstract

We propose a theory for the multi-ring pattern of the deposits that are formed when droplets of suspension are dried on a substrate. Assuming a standard model for the stick-slip motion of the contact line, we show that as droplets evaporate, many concentric rings of deposits are formed, but are taken over by a solid-circle pattern in the final stage of drying. An analytical expression is given to indicate when ring-pattern changes to solid-circle pattern during an evaporation process. The results are in qualitative agreement with existing experiments, and the other predictions on how the evaporation rate, droplet radius and receding contact angle affect the pattern are all subject to experimental test.

Keywords: Drop phenomenon, Evaporation, Contact line motion, Wetting, Onsager principle theory

* manxk@buaa.edu.cn

INTRODUCTION

When a droplet of suspension placed on a substrate is dried, it leaves various patterns of deposits on the substrate. A well-known pattern is the ring-like deposit left when a coffee droplet is dried on a plate. The deposition pattern has been studied for various combination of solutes, solvents, and surfaces, and a variety of patterns have been reported in the past [1–7].

In many situations, the deposits form concentric rings called multi-rings. This pattern has been observed in evaporating films [8], liquid droplets [9–11], and confined solutions [12–14]. Other types of patterns, spoke-like or eye-like patterns are also observed [15, 16]. Understanding the mechanism of such patterns are interesting not only from scientific view point, but also from a view point of applications, in connection to surface patterning of optical devices [17], biomacromolecular recognition [18] and disease detections [19, 20].

In this paper, we shall focus on the multi-ring pattern, and present a simple theory for the origin of this pattern. Multi-ring has been explained by the stick-slip motion of the contact line (CL). When the CL is pinned, a flow is created from the droplet center to its edge to supply the liquid to the edge. This flow convects solutes to the edge and deposits them near the CL. As the droplet volume decreases by evaporation, the contact angle decreases, and creates an inward unbalanced force (depinning force) acting on the contact line. When the contact angle becomes less than the receding contact angle θ_R (the angle at which the contact line starts to recede), the contact line starts to slip and move quickly towards the center until it becomes pinned again. The repetition of this stick-slip motion of the CL generates the multi-ring pattern.

Although the multi-ring formation has been explained qualitatively by this mechanism, theoretical modeling for the process has been undeveloped as the problem involves the fluid flow and the contact line motion in evaporating droplets coupled with the particle transport. Previous theoretical models [21–23] are written in the form of non-linear partial differential equations, and required numerical simulation to see the outcome of the model.

It has been reported that the multi-ring pattern is usually made of a solid circle in the center surrounded by many concentric rings, as schematically shown in Figure 1. This phenomenon has indeed been observed experimentally in drying of droplets containing a wide type of solutes, including colloid [1, 10, 24], polymer [11], DNA [2] and nanoparticles [25].

The open question that why and how a solid-circle often appears in the central region of concentric rings has not been answered as far as we know.

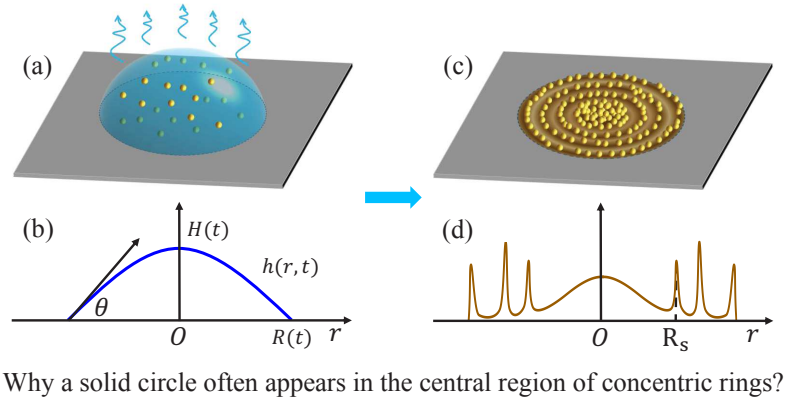


FIG. 1. Schematic of the multi-ring pattern. (a) A droplet of particle suspension is dried on a substrate. (b) Relevant parameters are the radius of the contact line R , the height of the droplet at the center H , and the contact angle θ . (c) The top view and (d) the side view of the deposition pattern. The deposit is made of a solid circle in the center of concentric rings. R_s is the radius of the innermost ring.

In this paper, we propose a simple model for the formation process of the multi-ring. This paper is an extension of our previous work [31, 35] on the contact line motion of an evaporating droplet. Using Onsager principle, we derived first-order ordinary differential equations for the droplet radius R and the contact angle θ , and have shown that the deposit pattern can change from ring-like (where the peak is a ring at the edge) to mountain like (where the peak is located at the center). To explain the change, we introduced a phenomenological parameter k_{cl} which represents the friction of the contact line, and is assumed to be a constant determined by the interaction between the liquid and substrate. In this paper, we assume that k_{cl} is not constant and changes with the contact angle. We will use the simplest possible model for k_{cl} to describe the stick-slip motion, and show that this model captures the characteristic features of the multi-ring pattern, and also can answer to the open question mentioned above. We also predict the condition for the multi-ring pattern to be observed, and address the key factors that determine the inter-ring spacing of the deposits.

THEORETICAL FRAMEWORK

Evolution Equations for Drying Droplets

We consider an evaporating droplet containing nonvolatile solutes, which is placed on a substrate. We assume that the droplet contact angle $\theta(t)$ is small ($\theta < 1$), and the surface profile of the droplet is given by (in a cylindrical coordinate)

$$h(r, t) = H(t) \left[1 - \frac{r^2}{R^2(t)} \right], \quad (1)$$

where $H(t)$ and $R(t)$ are the height and the radius of the droplet. The droplet volume $V(t)$ is then given by

$$V(t) = \frac{\pi}{4} \theta R^3(t). \quad (2)$$

Let R_0 , θ_0 and V_0 be the initial value of these parameters.

The droplet volume decreases in time by solvent evaporation. The rate \dot{V} is essentially determined by the diffusion of solvent vapor in air. When there is no air flow near the liquid surface, \dot{V} can be calculated by solving the diffusion equation of solvent vapor in air. Such studies [26, 27] have shown that \dot{V} is proportional to $R(t)$. Hence, we assume

$$\dot{V}(t) = \dot{V}_0 \frac{R(t)}{R_0}, \quad (3)$$

where the initial rate $\dot{V}_0 (< 0)$ is a constant determined by the initial droplet radius R_0 , the temperature and the humidity of the environment. The evaporation rate (the volume of solvent evaporating per unit time per unit surface area) is given by

$$J(t) = -\frac{\dot{V}(t)}{\pi R^2(t)} = -\frac{\dot{V}_0}{\pi R_0 R(t)}. \quad (4)$$

This indicates that the evaporation rate increases as droplet size $R(t)$ becomes small.

Given the volume evolution equation, we need one more equation either for $R(t)$ or $\theta(t)$ to describe the droplet shape evolution during evaporation. We determine the time evolution of these parameters by the Onsager principle [28, 29].

This principle is equivalent to the variational principle known in Stokesian hydrodynamics which states that the evolution of the system is determined by the minimum of Rayleighian defined by

$$\mathfrak{R} = \Phi + \dot{F} \quad (5)$$

where Φ is the energy dissipation function (the half of the energy dissipation rate created in the fluids by the boundary motion), and \dot{F} is the time derivative of the free energy of the system. The principle has been applied for the droplet motion by gravity [30] and by evaporation [31, 32].

We assume that the droplet is nearly flat [$R(t) \gg H(t)$] and use the lubrication approximation to calculate the dissipation function, which is written in the following form [31]

$$\Phi = \frac{3\pi^2\eta R^4}{4V} \left[\ln\left(\frac{R}{2\epsilon}\right) - 1 \right] \left(\dot{R} - \frac{R\dot{V}}{4V} \right)^2 + \pi\xi_{\text{cl}}R\dot{R}^2 \quad (6)$$

where η is the viscosity of the fluid, ξ_{cl} is a phenomenological parameter representing the mobility of the contact line, and ϵ being the molecular cut-off length which is introduced to remove the divergence in the energy dissipation at the contact line. The first term in Eq. (6) represents the usual hydrodynamic energy dissipation in the lubrication approximation, while the second term represents the extra energy dissipation associated with the contact line motion over substrate.

The free energy F is a sum of the interfacial energy by assuming the droplet size is less than the capillary length. The time derivative of such free energy is [31]

$$\dot{F} = \gamma_{LV} \left[\left(-\frac{16V^2}{\pi R^5} + \pi\theta_e^2 R \right) \dot{R} + \frac{8V\dot{V}}{\pi R^4} \right]. \quad (7)$$

where γ_{LV} is the liquid/vapor surface tension and θ_e is the equilibrium contact angle.

By minimizing the Rayleighian $\mathfrak{R} = \Phi + \dot{F}$ with respect to \dot{R} , we obtain the force balance equation for the contact line as

$$\xi_{\text{hydro}} \left(\dot{R} - \frac{R\dot{V}}{4V} \right) + \xi_{\text{cl}}\dot{R} = \frac{\gamma_{LV}}{2} (\theta^2 - \theta_e^2). \quad (8)$$

The right hand side represents the unbalanced capillary force acting on the contact line, where γ_{LV} is the surface tension, and θ_e is the equilibrium contact angle. The left hand side represents the frictional force acting on the moving contact line, where ξ_{hydro} is the friction constant calculated by hydrodynamics [33] and ξ_{cl} is the phenomenological parameter introduced to account for the contact line hysteresis. The hydrodynamic friction constant is expressed by the fluid viscosity η as $\xi_{\text{hydro}} = 3C\eta/\theta$, where $C = \ln(R/2\epsilon) - 1$ is a constant arising from the molecular length scale ϵ .

Equation (8) can be rewritten as the time evolution equation of the droplet contact radius

$$(1 + k_{\text{cl}}) \dot{R} = \frac{R\dot{V}}{4V} + \frac{\gamma_{LV}\theta(\theta^2 - \theta_e^2)}{6C\eta}, \quad (9)$$

where k_{cl} is defined by $k_{\text{cl}} = \xi_{\text{cl}}/\xi_{\text{hydro}}$ and represents the importance of the extra friction constant ξ_{cl} of the contact line relative to the normal hydrodynamic friction ξ_{hydro} . We use k_{cl} as a phenomenological parameter to distinguish the stick state (where $k_{\text{cl}} \rightarrow \infty$), and the slip state (where $k_{\text{cl}} \rightarrow 0$).

In the previous paper [31], we take k_{cl} as constant, but now we assume that it has two values, low value in the slip state and high value in the stick state, which is written as

$$k_{\text{cl}} = \begin{cases} 0 & \text{for } \theta \leq \theta_{\text{R}} \text{ or } \dot{\theta} > 0, \\ \alpha & \text{for } \theta > \theta_{\text{R}} \text{ and } \dot{\theta} \leq 0, \end{cases} \quad (10)$$

where θ_{R} is the receding contact angle (the angle below which the contact line starts to recede) and α is a constant representing the CL moving ability. We take $\alpha = 100$ for all calculations, which is large enough to make the CL stick. The contact line sticks when $k_{\text{cl}} = \alpha$, while it slips when $k_{\text{cl}} = 0$.

When R is pinned, θ decreases due to the evaporation. The deviation between $\theta(t)$ and θ_e generates a capillary force to pull the CL inwardly, but the CL remains stick as far as θ is larger than θ_{R} . When θ becomes smaller than θ_{R} , the CL starts to recede, and θ starts to increase. When θ becomes equal to its maximum value, $\dot{\theta}$ becomes equal to zero, and the contact line starts to be pinned. The repetition of this dynamics generates the stick-slip motion of the contact line.

To characterize the evaporation rate, we introduce another dimensionless parameter k_{ev} by $k_{\text{ev}} = \tau_{\text{re}}/\tau_{\text{ev}}$. Here, τ_{ev} is the evaporation time defined by $\tau_{\text{ev}} = V_0/|\dot{V}_0|$, and τ_{re} is the relaxation time defined by $\tau_{\text{re}} = \eta V_0^{\frac{1}{3}}/\gamma_{LV}\theta_e^3$. If k_{ev} is large, the relaxation time is much longer than the evaporation time, leading to that the droplet volume decreases much faster than the equilibration of the contact angle, therefore, θ becomes much smaller than θ_e . On the other hand, if k_{ev} is small, θ remains close to θ_e .

Equations (2), (3), (9), and (10) determine the time evolution of $V(t)$, $R(t)$ and $\theta(t)$. These equations can be solved for given values of dimensionless evaporation rate k_{ev} , and two contact angles θ_{R} and θ_e .

Deposition Mechanism

The distribution of the deposits left on the substrate can be calculated by using the time evolution equations of the droplet volume and contact radius. Since the diffusion of the

solute in radial direction can be ignored for macroscopic droplets [34], we can assume that the solute moves with the same velocity as the fluid as long as the solute is in the droplet. The height-averaged fluid velocity at position r and time t , $v(r, t)$, is obtained by solving the conservation equation $\dot{h} = -\nabla \cdot (vh) - J$, resulting in a simple expression as

$$v(r, t) = r \left(\frac{\dot{R}}{R} - \frac{\dot{V}}{4V} \right). \quad (11)$$

A fluid flow from center to edge is induced when $v > 0$. On the other hand, $v < 0$ indicates a fluid flow from the edge to droplet center. Consider the particles located at r_0 at time $t = 0$. Let $\tilde{r}(r_0, t)$ be the average position of the particles at time t . Since the particles are carried by the fluid flow with the velocity $v(r, t)$ given by Eq. (11), $\tilde{r}(r_0, t)$ satisfies the equation

$$\frac{\partial \tilde{r}}{\partial t} = \tilde{r} \left(\frac{\dot{R}}{R} - \frac{\dot{V}}{4V} \right) \quad (12)$$

At some time, the particles arrive at the contact line and are deposited there. This happens at time t_d when $\tilde{r}(r_0, t_d) = R(t_d)$. The amount of particles deposit at this point is then calculated by $\tilde{r}(r_0, t_d)$ as follows.

The total amount of solute which was originally contained in the region between r_0 and $r_0 + dr_0$ at time $t = 0$ is $2\pi r_0 h(r_0, 0) \phi_0 dr_0$. When this interval meets the CL, all solutes within this interval deposit in the region between \tilde{r} and $\tilde{r} + d\tilde{r}$. Therefore, the density of deposit at the position \tilde{r} is given by

$$\mu = h(r_0, 0) \phi_0 \frac{r_0}{\tilde{r}} \left(\frac{d\tilde{r}}{dr_0} \right)^{-1}. \quad (13)$$

Notice that both the defined deposition time t_d and position \tilde{r} are functions of r_0 . More details of the model and deposition mechanism can be found in the previous work [35].

RESULTS AND DISCUSSION

The Stick-Slip Motion and The Inter-Ring Spacing

Typical droplet shape evolutions calculated from the model are shown in Figure 2. Figure 2a shows that $R(t)$ decreases stepwise, while Figure 2b shows that θ oscillates between the equilibrium contact angle $\theta_e = 0.4$ and the receding contact angle $\theta_R = 0.2$. The stick period becomes shorter as droplet size gets smaller since the evaporation rate increases as

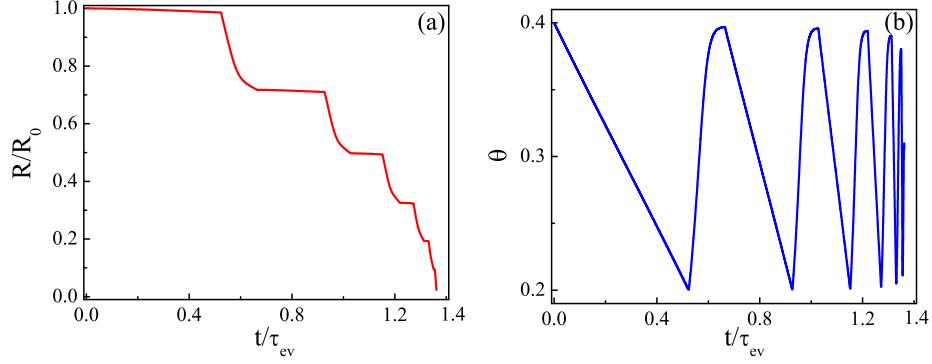


FIG. 2. Evolution of (a) the droplet contact line, $R(t)/R_0$, and (b) the droplet contact angle, θ , during an evaporation process. Here, the time is in units of τ_{ev} . The stick-slip motion of R is observed, while the contact angle oscillates between θ_e and θ_R . In both figures, the parameters are $k_{ev} = 10^{-3}$, $\theta_R = 0.2$, and $\theta_0 = \theta_e = 0.4$.

$R(t)$ decreases. In the final stage, the stick period gets so short that the CL looks to move continuously.

If the time evolution of the CL radius $R(t)$ is given, the profile of the deposit can be calculated by the method described in the subsection of deposition mechanism. Figure 3 shows how the deposition pattern changes when the receding contact angle θ_R is changed. Here the evaporation is assumed to be slow ($k_{ev} = 10^{-3}$), and $\theta_0 = \theta_e = 0.4$. It is seen that deposition pattern changes from coffee ring to multi-ring and to mountainlike by increasing θ_R from 0 to 0.4. When $\theta_R = 0$ (Fig. 3a), the CL remains stick since $\theta(t)$ stays larger than θ_R during evaporation, and coffee ring pattern is observed. When $\theta_R = \theta_e$ (Fig. 3f), the CL recedes freely, and creates the mountainlike pattern. Between these limits (Figs. 3b–3e), various multi-ring patterns are obtained. As θ_R increases, the number of rings increases and the inter-ring spacing ΔL decreases since the CL becomes easily depinned with the increase of θ_R . Figure 3 indicates that coffee ring and mountain-like patterns are special cases of multi-rings: they can be regarded as a multi-ring with $\Delta L \rightarrow \infty$ and $\Delta L \rightarrow 0$, respectively.

Figure 4 shows the inter-ring spacing ΔL as a function of the rescaled distance to the droplet center r/R_0 for different θ_R and k_{ev} . It is clear seen that ΔL is an increasing function of r/R_0 for all cases, indicating that rings are denser near the center than the edge. Figure 4a also shows that as θ_R increases, ΔL decreases and the number of rings increases, while Fig. 4b shows that as the evaporation rate k_{ev} increases, ΔL increases and the number

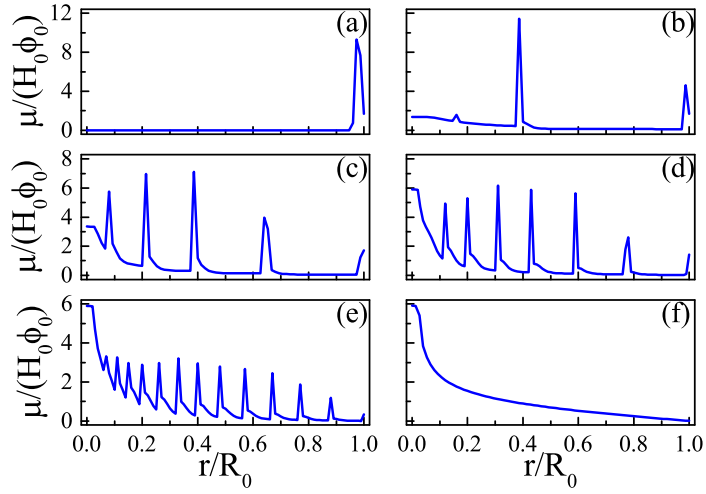


FIG. 3. Different profile of the deposits left on the substrate when the drying is completed for droplets with different values of θ_R , (a) $\theta_R = 0.00$; (b) $\theta_R = 0.08$; (c) $\theta_R = 0.16$; (d) $\theta_R = 0.24$; (e) $\theta_R = 0.32$; (f) $\theta_R = 0.4$. For all calculations, $\theta_0 = \theta_e = 0.4$, $R_0 = 4$, and $k_{ev} = 10^{-3}$.

of rings decreases.

Such tendencies have indeed been observed experimentally [13, 24]. Yang et al. [24] measured the distance between two successive rings and reported that ΔL decreases almost linearly with the radius $\Delta L \sim r$. The increase of ΔL as a function of the ring radius is also observed in different experimental set-ups. Xu et al. [13] studied the multi-ring pattern of polymer solutions evaporating between a sphere and a flat substrate. They showed that the center-to-center distance between adjacent rings is an increasing function of the distance from the touching point of the sphere on the substrate. In both cases, the inter-ring spacing varies with the ring radius, and is consistent with our theory.

The effects of θ_R and evaporation rate on ΔL are also consistent with experiments. Yang et al [24] showed that ΔL is larger for a larger particle volume fraction. They explained that this is due to the increase of pinning force with the increase of particle concentration. The pinning force is related to the receding contact angle θ_R in our model: the larger the pinning force is, the smaller the receding contact angle is. Figure 4a shows that ΔL indeed increases when θ_R decreases from 0.32 to 0.08, which is qualitatively consistent with the experimental results. On the other hand, Xu et al [13] showed that as the evaporation rate increases, the spacing ΔL increases, and the number of ring decreases. Figure 4b confirmed

this experimental finding, where each dot in this figure indicates one ring of the deposition pattern.

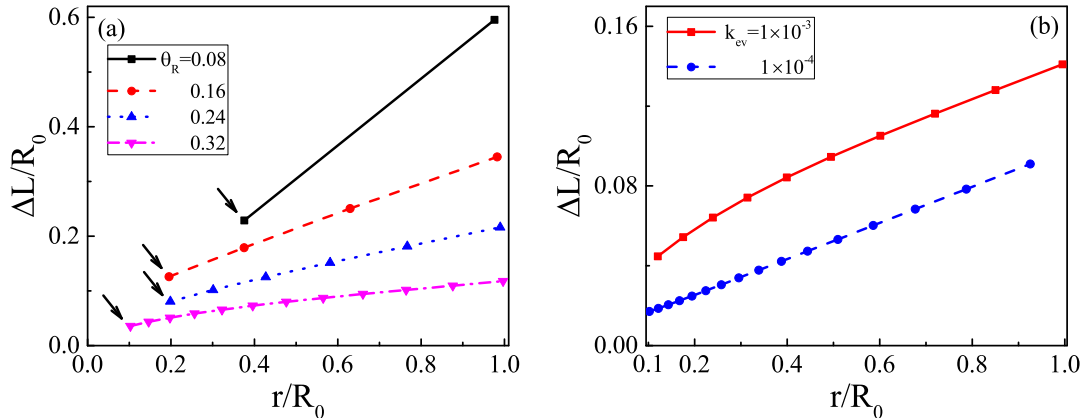


FIG. 4. The rescaled inter-ring spacing $\Delta L/R_0$ is plotted as a function of the distance to the droplet center r/R_0 for different θ_R and k_{ev} . (a) As the receding contact angle increases (or the contact angle hysteresis decreases), the total number of rings increases, while ΔL decreases. The vertical arrows indicate the radius of the last ring of the multi-ring pattern. The parameter $k_{ev} = 10^{-3}$. (b) As the evaporation rate (k_{ev}) increases, ΔL increases while the number of rings decreases. The parameter $\theta_R = 0.3$. For all cases, $\theta_e = \theta_0 = 0.4$.

ΔL can be estimated by the following simple argument. The CL starts to recede when θ becomes equal to θ_R and quickly moves to the next pinning point where $\dot{\theta}$ becomes equal to 0 (or θ becomes close to θ_e). Hence the volume conservation equation is written as

$$\frac{\pi}{4}\theta_R R^3 = \frac{\pi}{4}\theta_e (R - \Delta L)^3 + \Delta V. \quad (14)$$

where ΔV is the volume change of the droplet during the process. For slow evaporation, we may assume $\Delta V \ll V$, then Eq. (14) gives

$$\Delta L = R \left[1 - \left(\frac{\theta_R}{\theta_e} \right)^{\frac{1}{3}} \right]. \quad (15)$$

Equation (15) indicates that ΔL decreases as R decreases, but increases as θ_R decreases, which qualitatively agrees with the numerical results in Fig. 4a. It is interesting to note that Eq. (15) explains the formation of mountain-like and coffee ring patterns (since $\Delta L = 0$ for $\theta_R = \theta_e$ and $\Delta L = R_0$ for $\theta_R = 0$).

The Condition for Multi-Ring Formation

In the previous subsection, we have shown that for the multi-ring pattern to be observed, the contact line has to do stick-slip motion (i.e., switching between pinned state and depinned state). A condition for this to happen is that the receding contact angle θ_R is non-zero, but this is not the only condition for the stick-slip motion. In fact, the evaporation rate k_{ev} is another important factor, and its combined effects with θ_R in the condition for multi-ring formation can be estimated theoretically.

First we rewrite Eq. (9) for \dot{R} to an equation for $\dot{\theta}$:

$$(1 + k_{cl}) \tau_{re} \dot{\theta} = -\frac{k_{ev} (1 + 4k_{cl}) V_0}{\pi R_0 R^2} + \frac{V_0^{\frac{1}{3}} \theta^2 (\theta_e^2 - \theta^2)}{2C\theta_e^3 R}. \quad (16)$$

The first term on the right hand side is negative, while the second term is positive since θ is less than θ_e during the evaporation.

Now consider a droplet in the stick state. As solvent evaporates, the contact angle θ decreases (because k_{cl} is large in the stick state). When θ becomes equal to θ_R , k_{cl} switches from large positive value to 0. In the usual stick-slip motion, this jump of k_{cl} makes the right hand side positive, and θ starts to increase, which eventually causes the next stick of the CL. However, if the evaporation rate k_{ev} is large, the change of k_{cl} does not cause the sign change of $\dot{\theta}$, and θ keeps decreasing even in the slip state. If this happens, the contact line keeps receding until it reaches the center, and no ring appears. Whether the contact angle starts to increase or not when slip starts (i.e., when θ and k_{cl} become equal to θ_R and 0, respectively) depends on the sign of the right hand side of Eq. (16): if the sign is negative, the contact angle keeps decreasing, and no second ring appears, while if the sign is positive, the contact angle starts to increase, and will form next inner ring. The condition that multi-ring is observed is therefore given by

$$\theta_R^2 (\theta_e^2 - \theta_R^2) \geq C \left(\frac{\theta_0}{\sqrt{2\pi}} \right)^{\frac{2}{3}} \theta_e^3 k_{ev}, \quad (17)$$

where we have set R equal to R_0 and $k_{cl} = 0$. Equation (17) gives the condition for the multi-ring pattern to be observed for a droplet having initial radius R_0 and initial contact angle θ_0 (Notice that the condition depends on R_0 since k_{ev} depends on R_0).

Figure 5 shows the region defined by Eq. (17). Here θ_0 has been set to be equal to θ_e . A given droplet can form multi-ring pattern as long as its initial state is located in the region

of "multi-ring". The boundary is determined by the evaporation rate (characterized by k_{ev}) and the three contact angles (equilibrium angle, initial angle and receding angle). The figure indicates that multi-ring is not observed if the evaporation rate is large. It also shows that droplets with larger equilibrium contact angles have larger parameter space for multi-ring pattern. It should be noted that in this graph the mountain-like pattern is included in the category of "single-ring" since there is no inner ring in the mountain-like pattern.

Terminal Behavior of Multi-Ring

Figure 3 also shows that even if a droplet leaves many rings as it evaporates, the ring-pattern disappears in the final stage of drying. This is consistent with experimental observations [1, 2, 10, 11, 24, 25] that the multi-ring pattern is usually made of a solid circle in the center surrounded by many concentric rings. Here we discuss how the ring pattern changes to solid circle pattern, and estimate the radius of the innermost ring R_S .

We consider a 2D parameter space made of θ and R , and investigate the time evolution of the droplet state point (θ, R) during evaporation in this space. The contact line is in the stick state when k_{cl} is α (a large positive value), and in the slip state when k_{cl} is zero. The

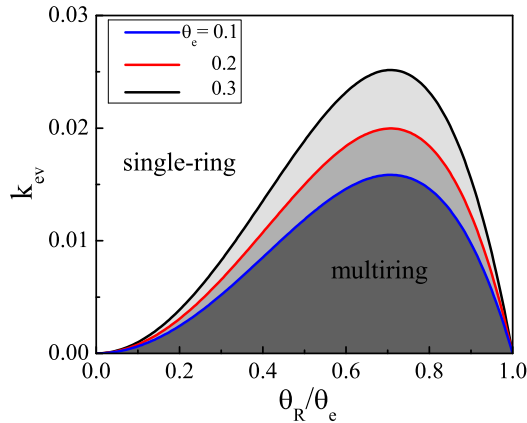


FIG. 5. Phase diagram for the multi-ring formation in the plane of the rescaled receding contact angle, θ_R/θ_e , and the evaporation rate, k_{ev} . The lines indicate the boundary between a multi-ring phase below and a single-ring phase above.

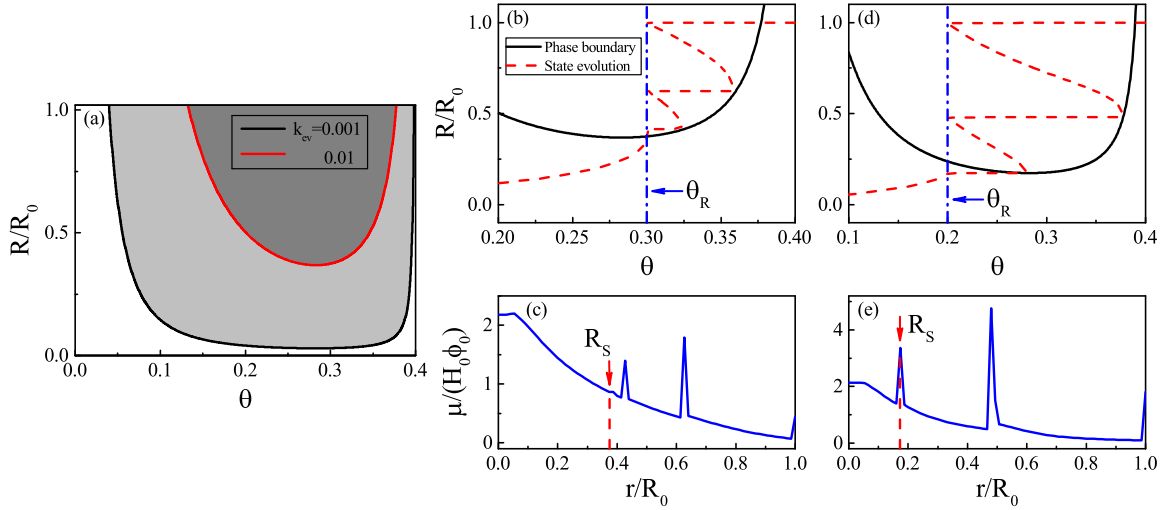


FIG. 6. Phase space of the dynamical model for evaporating droplet. The dark region shows the $\dot{\theta} > 0$ region for a droplet in depinned state. If a depinned droplet described by $(\theta, R/R_0)$ is located in this region, it will be pinned and form a ring. On the other hand, if the droplet is outside of this region, it will form a solid-circle instead. For Figs. (b) to (e): in both up column figures, the red dashed lines are the evolving trajectories of $\theta(t)$ and $R(t)$ of droplet, while the black solid lines denotes the boundary of $\dot{\theta} = 0$; Both down column figures are the corresponding deposition patterns. The arrows in Figs. (c) and (e) indicate the positions at which the multi-ring terminates. The calculation parameters are: $k_{ev} = 0.01$ and $\theta_R = 0.3$ in (b) and (c), and $k_{ev} = 0.005$ and $\theta_R = 0.2$ in (d) and (e), while $\theta_e = \theta_0 = 0.4$ for all figures.

transition from the stick state to the slip state takes place when

$$\theta = \theta_R. \quad (18)$$

On the other hand, the transition from the slip state to the stick state takes place when $\dot{\theta}$ given by Eq. (16) becomes zero, or R is equal to $g(\theta)$ defined by

$$g(\theta) = \frac{2C\theta_e^3 V_0^{\frac{2}{3}}}{\pi R_0} \frac{k_{ev}}{\theta^2 (\theta_e^2 - \theta^2)}. \quad (19)$$

The lines $R = g(\theta)$ are shown in Fig. 6a for two evaporation rates, $k_{ev} = 10^{-2}$ and $k_{ev} = 10^{-3}$. The line separates the $\dot{\theta} > 0$ region above and $\dot{\theta} < 0$ region below. This phase diagram shows that when the droplet contact line is in the slip state: if the state point

(θ, R) is in the $\dot{\theta} > 0$ region the contact angle increases until it arrives at the boundary line, where the slip-to-stick transition takes place resulting in the multi-ring pattern; If the state point is in the $\dot{\theta} < 0$ region, the contact line can not stick again resulting in the solid-circle pattern. It is shown that the range of parameter space for multi-ring formation is wider for slower evaporation ($k_{\text{ev}} = 10^{-3}$) than faster evaporation ($k_{\text{ev}} = 10^{-2}$).

These two lines $\theta = \theta_R$ and $R = g(\theta)$ in the (θ, R) space define a region $\theta > \theta_R$ and $R > g(\theta)$, which we shall call the oscillatory region. If the state point (θ, R) is in the oscillatory region, the point goes back and forth between the two lines and the stick-slip motion occurs, as shown in Figs. 6b and 6d by the red-dashed lines. In this case, multi-ring deposition pattern appears, where each ring corresponds to a stick state. If the state point (θ, R) moves out of the region, the stick-slip motion terminates leading to the termination of ring-pattern.

There are two ways for the state point to move out of the oscillatory region. Let θ_c be the angle at which $g(\theta)$ becomes minimum. Using Eq. (19), we have $\theta_c = \theta_e/\sqrt{2}$. If $\theta_R > \theta_c$, the state point moves out of the oscillatory region passing through the intersection of the two lines $\theta = \theta_R$ and $R = g(\theta)$ (see Fig. 6b). In this case, the radius R_S of the innermost ring is given by the R coordinate of the intersection, i.e., $R_S = g(\theta_R)$, or by use of Eq. (19)

$$R_S = \frac{2C\theta_e^3 V_0^{\frac{2}{3}} k_{\text{ev}}}{\pi R_0 \theta_R^2 (\theta_e^2 - \theta_R^2)}. \quad (20)$$

On the other hand, if $\theta_R < \theta_c$ the state point can be outside of the oscillatory region by moving out of the region $R > g(\theta)$ (see Fig. 6d). In this case, R_S is given by the radius of the last stick state, and depends on the initial state. We can use the minimum of the curve $R = g(\theta)$ to estimate R_S , i.e., $R_S \approx g(\theta_c)$. Using Eq. (19), we have

$$R_S = \frac{8CV_0^{\frac{2}{3}} k_{\text{ev}}}{\pi R_0 \theta_e}. \quad (21)$$

These theoretical values of R_S are shown by arrows in Figs. 6c and 6e, which are the deposition patterns of Fig. 6b and 6d, respectively. It is seen that they represent well the terminal point of the multi-ring pattern.

CONCLUSION

In this paper, we have proposed a simple model for the formation of the multi-ring pattern that is often observed in drying droplets. The model predicts that the multi-ring pattern appears only when the evaporation rate is less than a certain critical value determined by the equilibrium contact angle θ_e and the receding contact angle θ_R . The model shows that as the ring radius decreases and below a critical value (the innermost ring radius), the multi-ring is replaced by a solid-circle pattern. Analytical expressions have been given for the radius of the innermost ring in terms of θ_e , θ_R and the evaporation rate. These results agree with existing experiments qualitatively, and can be tested quantitatively. The remaining question is how the key parameters in the model changes with the solute details (concentration [2, 4], particle size [10, 18] and shape [36, 37] etc), and such effects will be discussed in future.

Acknowledgement. This work was supported in part by Grant No. 21434001 and 21404003 of the National Natural Science Foundation of China (NSFC), the joint NSFC-ISF Research Program, jointly funded by the NSFC under Grant No. 51561145002 and the Israel Science Foundation (ISF) under Grant No. 885/15, and the Fundamental Research Funds for the Central Universities.

REFERENCES

- [1] Adachi, E.; Dimitrov, A. S.; Nagayama, K. Stripe patterns formed on a glass surface during droplet evaporation. *Langmuir* **1995**, *11*, 1057-1060.
- [2] Maheshwari, S.; Zhang, L.; Zhu, Y. X.; Chang, H. C. Coupling between precipitation and contact-line dynamics: multiring stains and stick-slip motion. *Phys. Rev. Lett.* **2008**, *100*, 044503.
- [3] Moffat, J. R.; Sefiane, K.; Shanahan, M. E. R. Effect of TiO₂ nanoparticles on contact line stick-slip behavior of volatile drops. *J. Phys. Chem. B* **2009**, *113*, 8860-8866.
- [4] Orejon, D.; Sefiane, K.; Shanahan, M. E. R. Stick-slip of evaporating droplets: substrate hydrophobicity and nanoparticle concentration. *Langmuir* **2011**, *27*, 12834-12843.
- [5] Seo, C.; Jang, D.; Chae, J.; Shin, S. Altering the coffee-ring effect by adding a surfactant-like viscous polymer solution. *Sci. Rep.* **2017**, *7*, 500.
- [6] Giorgiutti-Dauphiné, F.; Pauchard, L. Drying drops containing solutes: from hydrodynamical to mechanical instabilities. *Eur. Phys. J. E* **2018**, *41*, 32.
- [7] Tarafdar, S.; Tarasevich, Y. Y.; Choudhury, M. D.; Dutta, T.; Zang, D. Y. Droplet drying patterns on solid substrates: from hydrophilic to super hydrophobic contact to levitating drops. *Adv. Condens. Matter Phys.* **2018**, *2018*, 5214924.
- [8] Xia, Y.; Kim, E.; Mrksich, M.; Whitesides, G. M. Microcontact printing of alkanethiols on copper and its application in microfabrication. *Chem. Mater.* **1996**, *8*, 601-603.
- [9] Deegan, R. D. Pattern formation in drying drops. *Phys. Rev. E* **2000**, *61*, 475-485.
- [10] Shmuylovich, L.; Shen, A. Q.; Stone, H. A. Surface morphology of drying latex films: multiple ring formation. *Langmuir* **2002**, *18*, 3441-3445.
- [11] Bi, W. G.; Wu, X. Y.; Yeow, E. K. L. Unconventional multiple ring structure formation from evaporation-induced self-assembly of polymers. *Langmuir* **2012**, *28*, 11056-11063.
- [12] Lin, Z. Q.; Granick, S. Patterns formed by droplet evaporation from a restricted geometry. *J. Am. Chem. Soc.* **2005**, *127*, 2816-2817.
- [13] Xu, J.; Xia, J. F.; Hong, S. W.; Lin, Z. Q.; Qiu, F.; Yang, Y. L. Self-assembly of gradient concentric rings via solvent evaporation from a capillary bridge. *Phys. Rev. Lett.* **2006**, *96*,

066104.

- [14] Han, W.; Lin, Z. Q. Learning from "coffee rings": ordered structures enabled by controlled evaporative self-assembly. *Angew. Chem. Int. Ed.* **2012**, *51*, 1534-1546.
- [15] Zhang, Y.; Qian, Y.; Liu, Z.; Li, Z.; Zang, D. Surface wrinkling and cracking dynamics in the drying of colloidal droplets. *Eur. Phys. J. E.* **2014**, *37*, 84.
- [16] Li, Y.; Lv, C.; Li, Z.; Quéré, D.; Zheng, Q. From coffee rings to coffee eyes. *Soft Matter* **2015**, *11*, 4669-4673.
- [17] Derby, B. Inkjet printing of functional and structural materials: fluid property requirements, feature stability, and resolution. *Annu. Rev. Mater. Res.* **2010**, *40*, 395-414.
- [18] Zhang, L.; Maheshwari, S.; Chang, H. C.; Zhu, Y. X. Evaporative self-assembly from complex DNA-colloid suspensions. *Langmuir* **2008**, *24*, 3911-3917.
- [19] Yakhno, T. A.; et al. The informative-capacity phenomenon of drying drops. *IEEE Eng. Med. Biol. Mag.* **2005**, *24*, 96-104.
- [20] Trantum, J. R.; Wright, D. W.; Haselton, F. R. Biomarker-mediated disruption of coffee-ring formation as a low resource diagnostic indicator. *Langmuir* **2012**, *28*, 2187-2193.
- [21] Nonomura, M.; Kobayashi, R.; Nishiura, Y.; Shimomura, M. Periodic precipitation during droplet evaporation on a substrate. *J. Phys. Soc. Jpn.* **2003**, *72*, 2468-2471.
- [22] Frastia, L.; Archer, A. J.; Thiele, U. Dynamical model for the formation of patterned deposits at receding contact lines. *Phys. Rev. Lett.* **2011**, *106*, 077801.
- [23] Zigelman, A.; Manor, O. A model for pattern deposition from an evaporating solution subject to contact angle hysteresis and finite solubility. *Soft Matter* **2016**, *12*, 5693-5707.
- [24] Yang, X.; Li, C. Y.; Sun, Y. From multi-ring to spider web and radial spoke: competition between the receding contact line and particle deposition in a drying colloidal drop. *Soft Matter* **2014**, *10*, 4458-4463.
- [25] Li, H.; et al. Direct observation of nanoparticle multiple-ring pattern formation during droplet evaporation with dark-field microscopy. *Phys. Chem. Chem. Phys.* **2016**, *18*, 13018-13025.
- [26] Parisse, F.; Allain, C. Drying of colloidal suspension droplets: experimental study and profile renormalization. *Langmuir* **1997**, *13*, 3598-3602.
- [27] Kobayashi, M.; Makino, M.; Okuzono, T.; Doi, M. Interference effects in the drying of polymer droplets on substrate. *J. Phys. Soc. Jpn.* **2010**, *79*, 044802.
- [28] Doi, M. *Soft Matter Physics*; Oxford University Press, 2013.

- [29] Doi, M. Onsager principle as a tool for approximation. *Chin. Phys. B* **2015**, *24*, 020505.
- [30] Xu, X. M.; Di, Y. N.; Doi, M. Variational method for liquids moving on a substrate. *Phys. Fluids* **2016**, *28*, 087101.
- [31] Man, X. K.; Doi, M. Ring to mountain transition in deposition pattern of drying droplets. *Phys. Rev. Lett.* **2016**, *116*, 066101.
- [32] Man, X. K.; Doi, M. Vapor-induced motion of liquid droplets on an inert substrate. *Phys. Rev. Lett.* **2017**, *119*, 044502.
- [33] Bonn, D.; Eggers, J.; Indekeu, J.; Meunier, J.; Rolley, E. Wetting and spreading. *Rev. Mod. Phys.* **2009**, *81*, 739-805.
- [34] Anderson, D. M.; Davis, S. H. The spreading of volatile liquid droplets on heated surfaces. *Phys. Fluids* **1995**, *7*, 248-265.
- [35] Hu, S. Y.; Wang, Y. H.; Man, X. K.; Doi, M. Deposition patterns of two neighboring droplets: Onsager variational principle studies. *Langmuir* **2017**, *33*, 5965-5972.
- [36] Yunker, P. J.; Still, T.; Lohr, M. A.; Yodh, A. G. Suppression of the coffee-ring effect by shape-dependent capillary interactions. *Nature* **2011**, *476*, 308-311.
- [37] Askounis, A.; Sefiane, K.; Koutsos, V.; Shanahan, M. E. R. Effect of particle geometry on triple line motion of nano-fluid drops and deposit nano-structuring. *Adv. Colloid Inter. Sci.* **2015**, *222*, 44-57.

for Table of Contents use only

Multi-Ring Deposition Pattern of Drying Droplets

Mengmeng Wu, Xingkun Man, and Masao Doi

